Nano Research 2016, 9(4): 942–950
DOI 10.1007/s12274-015-0980-y
Research Article
ISSN 1998-0124
CN 11-5974/O4

Converting ultrafine silver nanoclusters to monodisperse silver sulfide nanoparticles via a reversible phase transfer protocol

Yan Feng[1,2], Qiaofeng Yao[2], Jingguo Li[2], Nirmal Goswami[2], Jianping Xie[2] (✉), and Jun Yang[1] (✉)

[1] *State Key Laboratory of Multiphase Complex Systems, Institute of Process Engineering, Chinese Academy of Sciences, Beijing 100190, China*
[2] *Department of Chemical and Biomolecular Engineering, National University of Singapore, 10 Kent Ridge Crescent, Singapore 119260, Singapore*

Received: 28 October 2015
Revised: 14 December 2015
Accepted: 15 December 2015

KEYWORDS
silver sulfide nanoparticles, silver nanoclusters, thiolated metal nanoclusters, two-phase synthesis

ABSTRACT

To achieve better control of the formation of silver sulfide (Ag_2S) nanoparticles, ultrasmall Ag nanoclusters protected by thiolate ligands ($Ag_{44}(SR)_{30}$ and $Ag_{16}(GSH)_9$) are used as precursors, which, via delicate chemistry, can be readily converted to monodisperse Ag_2S nanoparticles with controllable sizes (4–16 nm) and switchable solvent affinity (between aqueous and organic solvents). This new synthetic protocol makes use of the atomic monodispersity and rich surface chemistry of Ag nanoclusters and a novel two-phase protocol design, which results in a well-controlled reaction environment for the formation of Ag_2S nanoparticles.

1 Introduction

Silver sulfide nanoparticles (Ag_2S NPs), which have a bulk band gap of 1.1 eV and a relatively large absorption coefficient, have recently emerged as a popular class of semiconductor nanocrystals in the research community due to their good photoelectric and thermoelectric properties, finding increasing use in the design of optics, electronics, and near-infrared (NIR) fluorescent probes [1–5]. In addition, Ag_2S NPs can be combined with other functional materials to improve their suitability for various applications. For example, Ag_2S NPs have been incorporated into a semiconductor-metal nanocomposite, showing good catalytic activity for methanol oxidation at room temperature [6]. Size and surface structure are two important factors that determine the physicochemical properties of Ag_2S NPs, as well as their performance in various applications. This has motivated the community to develop efficient synthetic strategies

Address correspondence to Jianping Xie, chexiej@nus.edu.sg; Jun Yang, jyang@ipe.ac.cn

for the preparation of Ag_2S NPs with well-controlled sizes and good dispersions in solution.

A number of methods have been recently developed for the synthesis of Ag_2S NPs [7–9]. The reported protocols are typically carried out in organic solvent and at a relatively high temperature, through the reaction of monodisperse Ag NPs with sulfur in solution, often with the use of expensive and unstable organometallic precursors [1, 3–5]. While these protocols yield monodisperse Ag_2S NPs in organic solvents, they are less successful when preparing Ag_2S NPs in aqueous solution. In particular, the poor solubility of S in water and the relatively polydisperse nature of many water-soluble Ag NP precursors often led to adverse effects on the homogeneous growth of Ag_2S NPs, forming polydisperse Ag_2S NPs in water. Another approach to the synthesis of water-soluble Ag_2S NPs uses the reaction between Ag^+ and S^{2-} in the aqueous phase. A number of Ag_2S NPs have been successfully synthesized using this reaction in the presence of different protecting agents, such as proteins [10, 11], polymers [12], and bis(p-sulfonatophenyl)phenylphosphine (BSPP) [6]. However, the fast reaction kinetics between Ag^+ and S^{2-} in water makes the separation of the nucleation and growth of Ag_2S NPs difficult, and according to the general "nucleation-growth" scheme, the effective separation of nucleation and growth of nanocrystals is crucial for the preparation of monodisperse NPs. Therefore, although monodisperse water-soluble Ag_2S NPs with various sizes are of interest for many applications (e.g., biomedical), their development has been largely curtailed by the lack of efficient synthetic protocols.

Such a synthetic challenge could be addressed by using another maturing class of particles, so-called nanoclusters (NCs), as the precursors. Noble metal (e.g., Au and Ag) NCs are a family of ultrafine particles with core sizes smaller than 2 nm [13–15]. They often display unique physical and chemical properties that are distinctively different from both single metal atoms and relatively large metal NPs (>2 nm), and thus have potential applications in various fields including biomedicine, environmental monitoring, and catalysis [16–23]. Thanks to recent advances in cluster chemistry, Au and Ag NCs can now be prepared with well-controlled sizes, compositions, and surface chemistry (often at atomic levels of precision) [24–32]. Ag NCs could be a good source for the preparation of Ag_2S NPs for two reasons. First, their atomic monodispersity, which may not be present in the Ag NP precursors, could readily transfer to good monodispersity of Ag_2S NPs. Second, the rich surface chemistry of Ag NCs could provide an efficient way to regulate the formation kinetics of Ag_2S NPs, thus facilitating their conversion to monodisperse Ag_2S NPs.

In this study, we report an Ag-NC-based phase-transfer assisted method for the preparation of monodisperse Ag_2S NPs with controllable size and surface chemistry. The synthesis processes are illustrated in Fig. 1. In the first step, water-soluble Ag NCs ($Ag_{44}(SR)_{30}$ or $Ag_{16}(GSH)_9$) with negative charges were prepared in water, followed by phase transfer to an organic solvent (e.g., toluene) via formation of a hydrophobic monolayer of cetyltrimethylammonium cations (CTA^+) on the NC surface. In the second step, the phase-transferred Ag NCs reacted with S in the organic phase, leading to the formation of monodisperse Ag_2S NPs. As both S and phase-transferred Ag NCs were well dispersed in the organic phase, this phase transfer design gave a homogenous microenvironment for the formation of Ag_2S NPs. In addition, the outer layer of CTA^+ on the phase-transferred Ag NCs could serve as a mass transfer barrier for S, regulating its reaction kinetics with the Ag core of the NCs. A uniform and controllable environment was thus formed, resulting in the formation of Ag_2S NPs with good monodispersity and tailorable sizes (by adjusting the reaction kinetics). Furthermore, the mild reaction allowed Ag_2S NPs to retain the surface chemistry of their parent Ag NCs, i.e., reversible solubility in organic and aqueous phases by binding with or removal of CTA^+.

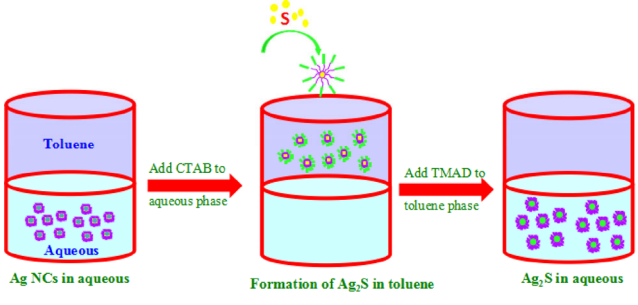

Figure 1 Schematic illustration of the synthesis of monodisperse Ag_2S NPs via a reversible phase transfer protocol.

2 Experimental

2.1 Chemicals

All chemicals are commercially available, and were purchased from the following suppliers: silver nitrate ($AgNO_3$) from Merck; p-mercaptobenzoic acid (p-MBA), caesium hydroxide (CsOH), L-glutathione reduced (GSH), sulfur, sodium borohydride ($NaBH_4$), sodium hydroxide (NaOH), cetyltrimethylammonium bromide (CTAB), tetramethylammonium hydroxide pentahydrate (TMAH), and decanoic acid (DA) from Sigma-Aldrich; and ethanol, methanol, and toluene from Tedia. All were used as received. All glassware was washed with aqua regia (HCl/HNO_3 in a 3:1 ratio by volume. Caution! Aqua regia is a very corrosive oxidizing agent that should be handled with great care) and rinsed with ethanol and ultrapure water before use. Ultrapure water with resistivity of 18.2 MΩ·cm^{-1} was used throughout the experiments.

2.2 Synthesis of Ag_{44}(p-MBA)$_{30}$

Ag_{44}(p-MBA)$_{30}$ was prepared according to published protocols [33, 34]. In a typical synthesis of Ag_{44}(p-MBA)$_{30}$, an aqueous $AgNO_3$ solution (2.6 mL, 11.9 mM) was mixed with an ethanolic p-MBA solution (1.5 mL, 83 mM), which led to the formation of insoluble precursors. The solution pH was then adjusted to 13.5 by introducing 100 μL of aqueous CsOH (50% *w*/*w*). Following this, an aqueous $NaBH_4$ solution (1.12 mL, 278 mM in 0.2 M CsOH) was added dropwise under vigorous stirring, and the solution was incubated at 50 °C for 10 h. The solution changed color from light yellow, to dark yellow, gray, and finally dark red. The dark red solution was collected as the final product.

2.3 Synthesis of $Ag_{16}(GSH)_9$

$Ag_{16}(GSH)_9$ was synthesized according to our reported protocol [19]. Aqueous solutions of $AgNO_3$ (20 mM) and GSH (50 mM) were first prepared with ultrapure water. An aqueous solution of $NaBH_4$ (112 mM) was also freshly prepared by dissolving 43 mg of $NaBH_4$ in 8 mL of ultrapure water, and then 2 mL of 1 M NaOH solution was introduced to the $NaBH_4$ solution. In a typical synthesis of GSH-protected Ag NC intermediates, aqueous solutions of GSH (150 μL, 50 mM), $AgNO_3$ (125 μL, 20 mM), and $NaBH_4$ (50 μL, 112 mM) were sequentially added to water (4.85 mL) under vigorous stirring. After 5 min, a deep red solution of Ag NC intermediates was collected. The as-prepared GSH-protected Ag NC intermediates were incubated at room temperature for 3 h. The deep red solution gradually changed to colorless, suggesting the formation of thiolate–Ag(I) complexes. Following this, an aqueous $NaBH_4$ solution (50 μL, 112 mM) was added to the colorless thiolate–Ag(I) solution under vigorous stirring. After 15 min, a light brown solution of Ag clusters formed. Without stirring, this solution was incubated at room temperature for 8 h, leading to the formation of $Ag_{16}(GSH)_9$ NCs.

2.4 Phase transfer of Ag NCs from aqueous to toluene

To transfer Ag NCs from water to toluene, an ethanolic CTAB solution (5 mL, 100 mM) was first introduced to the as-prepared Ag NC solution. The mixed solution was stirred for 20 s, leading to the formation of CTAB-coated p-MBA- or GSH-Ag NCs. Toluene (5 mL) was then added, and the mixed solution was stirred continuously for 1 min. After standing for 5 min, the CTAB-coated NCs were completely transferred to toluene.

2.5 Synthesis of Ag_2S NPs with different sizes

The phase-transferred Ag NCs (5 mL) and toluene (5 mL) were prepared in four 20-mL disposable glass vials. In a typical synthesis of Ag_2S NPs, 0.5 mg·mL^{-1} sulfur solution was prepared by adding 7.5 mg sulfur to toluene (15 mL). This sulfur solution was then introduced to the four vials at the Ag/S molar ratio of 4/1, 2/1, 1/1, and 1/2, respectively.

2.6 Phase transfer of Ag_2S NPs from toluene to aqueous solution

Hydrophobic tetramethylammonium decanoate (TMAD) was used to transfer the Ag_2S NPs back to water. A methanolic TMAD solution was first prepared by dissolving DA (1.7 g) and TMAH (1.8 g) in methanol (100 mL). In a typical phase transfer process, water (5 mL) and TMAD (5 mL) were sequentially added to the Ag_2S NPs in toluene (5 mL). The mixed solution

was stirred for 1 min, and the Ag_2S NPs were transferred back to water. The Ag_2S NP hydrosol was obtained by removing toluene.

2.7 Materials characterization

UV–vis absorption spectra were recorded on a Shimadzu UV-1800 spectrometer. Transmission electron microscopy (TEM) was performed on a JEOL JEM-2010 microscope operating at 200 kV. X-ray photoelectron spectra (XPS) were acquired on a Kratos AXIS UltraDLD spectrometer. Powder X-ray diffraction (XRD) patterns were collected on a Rigaku D/Max-3B diffractometer, using Cu Kα radiation (λ = 1.54056 Å).

3 Results and discussion

As a proof-of-concept, we used an ultrastable Ag_{44}(p-MBA)$_{30}$ NC as the starting material for Ag_2S NP synthesis, where p-MBA is p-mercaptobenzoic acid and the subscripts in the formula indicate the number of silver atoms and p-MBA ligands per cluster, respectively [33]. As displayed in Fig. S1 (in the Electronic Supplementary Material (ESM)), the Ag_{44}(p-MBA)$_{30}$ NCs were successfully prepared in the aqueous phase according to a reported protocol [34]. At neutral pH or above, p-MBA ligands acquire negative charges by deprotonation of the carboxyl group, which provides a means to develop a high density of negative charge on the surface of Ag_{44}(p-MBA)$_{30}$ NCs. These negatively charged Ag_{44}(p-MBA)$_{30}$ NCs then reacted with hydrophobic cations (e.g., CTA^+) in a biphasic water-toluene mixture. After 5 min vigorous stirring (1,000 rpm), Ag_{44}(p-MBA)$_{30}$ NCs were transferred from the aqueous phase to toluene due to the hydrophobicity provided by the hydrocarbon tail of CTA^+ [8, 35]. The successful transfer of Ag_{44}(p-MBA)$_{30}$ NCs was clearly

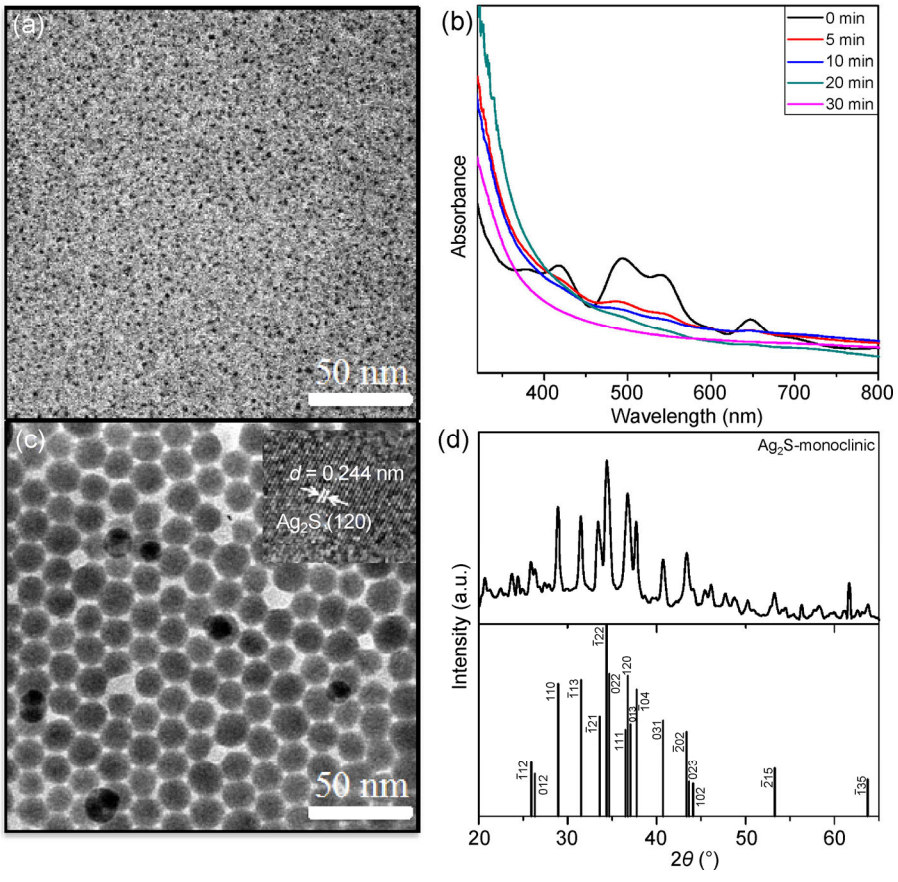

Figure 2 (a) TEM image of Ag_{44}(p-MBA)$_{30}$ NCs after transfer to toluene. (b) UV–vis absorption spectra of the Ag_{44}(p-MBA)$_{30}$ solution in toluene at different times after the addition of sulfur (0–30 min). (c) TEM image of the as-synthesized Ag_2S NPs. Inset is a high-resolution TEM image of a single Ag_2S particle. (d) XRD patterns of the as-synthesized Ag_2S NPs (top) and the standard reference of α-monoclinic Ag_2S (bottom).

seen from the transfer of the dark red color (typical of $Ag_{44}(SR)_{30}$ NCs, SR denotes thiolate ligand) from the aqueous to the organic phase (Fig. S1(b) in the ESM).

In addition, UV–vis absorption spectroscopy was also used to evaluate the effectiveness of the phase transfer. The phase-transferred Ag_{44}(p-MBA)$_{30}$ NCs showed characteristic absorption features of pure $Ag_{44}(SR)_{30}$ NCs at 374, 411, 483, 535, and 641 nm (Fig. 2(b), 0 min), which also suggests that the phase transfer process was a "soft" process that did not disrupt the size and structure of the NCs [36]. TEM images (Fig. 2(a)) confirmed the small size (<2 nm) and monodispersity of the phase-transferred Ag_{44}(p-MBA)$_{30}$ NCs.

The formation of Ag_2S NPs was triggered by mixing S with the phase-transferred Ag_{44}(p-MBA)$_{30}$ NCs in toluene. After stirring at 1,000 rpm for 30 min, monodisperse Ag_2S NPs were obtained, as shown by the color change of the solution (Fig. S1(c) in the ESM). At a feeding Ag/S ratio of 1/2, well-dispersed spherical Ag_2S NPs were produced (Fig. 2(c)) with a particle size of 16 nm. The inset of Fig. 2(c) shows a high-resolution TEM (HR-TEM) image of a typical Ag_2S NP. The crystal lattice fringes with a *d*-spacing of 0.244 nm can be indexed to the (120) facet of α-monoclinic Ag_2S, implying that the as-prepared NPs were high quality α-monoclinic crystalline Ag_2S. A similar conclusion can also be reached from the XRD data. As depicted in Fig. 2(d), all peaks in the XRD patterns of the as-prepared Ag_2S NPs can be indexed to α-monoclinic Ag_2S (JCPDS card 14-0072). The absence of Ag NPs and Ag(I)-thiolate complexes was also confirmed by XRD, suggesting a high yield of α-monoclinic Ag_2S NPs. The high conversion from Ag_{44}(p-MBA)$_{30}$ NCs to Ag_2S NPs is further supported by the time-evolution UV–vis absorption data. As the reaction proceeded, the characteristic absorption peaks of Ag_{44}(p-MBA)$_{30}$ NCs gradually faded while a featureless UV–vis absorption spectrum (typical of Ag_2S NPs) developed (Fig. 2(b)), suggesting that Ag_2S NPs were formed at the expense of Ag_{44}(p-MBA)$_{30}$ NCs. The absence of Ag_{44}(p-MBA)$_{30}$ NC absorption features in the final product (t = 30 min) suggests complete conversion from Ag_{44}(p-MBA)$_{30}$ NCs to Ag_2S NPs.

Other evidence of the formation of high quality Ag_2S NPs was provided by XPS and energy-dispersive X-ray spectroscopy (EDX). As shown in Fig. S2 (in the ESM), the binding energies of Ag $3d_{5/2}$ and $3d_{3/2}$ are 368.3 and 374.3 eV, respectively. This data confirmed that the Ag component in the final product was in the oxidized state [37], which is in good agreement with the formation of Ag_2S NPs. In addition, the EDX data (Fig. S3 in the ESM) suggests that the as-synthesized Ag_2S NPs had an atomic ratio of Ag/S = 1.8/1, close to the stoichiometry of bulk Ag_2S.

The formation of monodisperse Ag_2S NPs should be attributed to the mild, homogeneous, and controllable reaction environment for Ag_2S NP growth. The uniformity of the reaction environment was created by the combined implementation of atomically monodisperse precursor (e.g., Ag_{44}(p-MBA)$_{30}$ NCs) and the two-phase design, which allowed all reactants to be solubilized and well-mixed. It is worth noting that the monolayer of CTA^+ formed on the NC surface not only facilitated the phase transfer of Ag_{44}(p-MBA)$_{30}$ NCs, but also provided a mass transfer barrier to S in toluene. Owing to the decreased diffusion of S from the bulk to the Ag core of the Ag_{44}(p-MBA)$_{30}$ NCs, the reaction kinetics between S and Ag could be effectively controlled, allowing the formation of monodisperse Ag_2S NPs.

Moreover, the diffusion-controlled mechanism also provided a good way to tailor the size of the Ag_2S NPs. Previous studies suggest that rapid formation kinetics often favors the formation of large Ag_2S NPs [38–40]. Therefore, we reasoned that a simple change in the feeding concentration of S might alter the diffusion dynamics of S, thus modulating the formation kinetics of Ag_2S NPs, which could allow control of Ag_2S NPs size. To test this assumption, syntheses of Ag_2S NPs at different Ag/S molar ratio were carried out. Figures 3(a)–3(d) show the TEM images of Ag_2S NPs synthesized at Ag/S molar ratios of 4/1, 2/1, 1/1, and 1/2, respectively. As illustrated by the size histograms (Figs. 3(e)–3(h)), the average size of the Ag_2S NPs increased from 4 to 16 nm (with almost no change in monodispersity) as the Ag/S molar ratio decreased. The difference in particle sizes could also be seen in the colors of the as-synthesized Ag_2S NPs in toluene. As shown in Fig. 3 (insets), as particle size increased, the color of the Ag_2S solution changed from

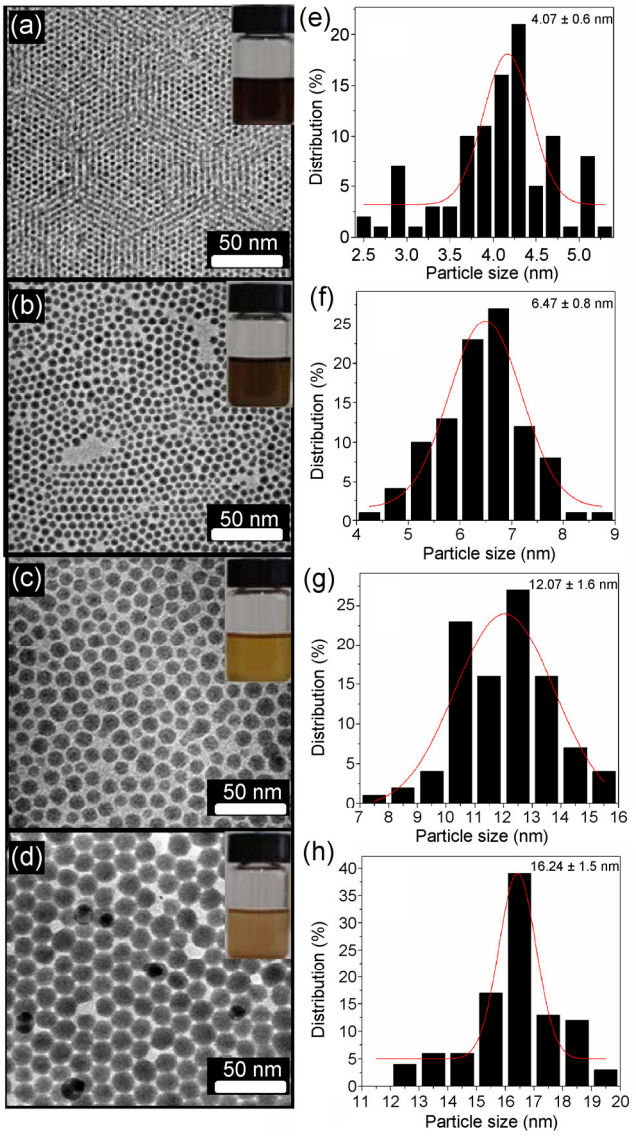

Figure 3 (a)–(d) TEM images (inset: photograph) and (e)–(h) histograms of Ag_2S NPs synthesized with Ag/S molar ratios of ((a) and (e)) 4/1, ((b) and (f)) 2/1, ((c) and (g)) 1/1, and ((d) and (h)) 1/2.

dark brown to light brown, both of which are different from the dark red of the original Ag_{44}(p-MBA)$_{30}$ NC solution.

Another salient feature of our Ag-NC-based phase-transfer assisted synthesis method is the tailorability of surface chemistry. Under the mild reaction kinetics established in toluene, the surface chemistry of the parent Ag_{44}(p-MBA)$_{30}$ NCs should be retained in Ag_2S NPs, i.e., the toluene-soluble Ag_2S NPs should be capped by CTA^+ bound p-MBA or p-MBA···CTA ligands. The electrostatic binding between p-MBA and CTA^+ thus provides a good mechanism for further tailoring the surface chemistry. Specifically, TMA···p-MBA-capped Ag_2S NPs and (CTA^+)D were formed by the ion-exchange reaction between p-MBA···CTA-capped Ag_2S NPs and TMAD. The more hydrophilic p-MBA···TMA-capped Ag_2S NPs could then transfer back to the aqueous phase while the more hydrophobic (CTA^+)D stayed in toluene. The FTIR spectrum of the Ag_2S NPs transferred to the aqueous phase (Fig. S4(c) in the ESM) was similar to that of the original Ag_{44}(p-MBA)$_{30}$ NCs (Fig. S4(b) in the ESM) and pure p-MBA (Fig. S4(a) in the ESM), suggesting that the water-soluble Ag_2S NPs were protected by p-MBA ligands. This phase transfer process is shown in Fig. S1(d) (in the ESM). The aqueous solution of Ag_2S NPs was highly stable, and no aggregates were observed even after weeks of storage at room temperature.

Since the Ag-NC-based phase-transfer assisted approach only requires the Ag NC precursors to be negatively charged, it should be generally applicable to other atomically precise Ag NCs with negatively charged surfaces. In order to test the feasibility of this approach with Ag NCs, we prepared a GSH-protected Ag NC, $Ag_{16}(GSH)_9$ [19], where a negatively charged surface could be easily achieved by the deprotonation of GSH at neutral or higher pH. A representative TEM

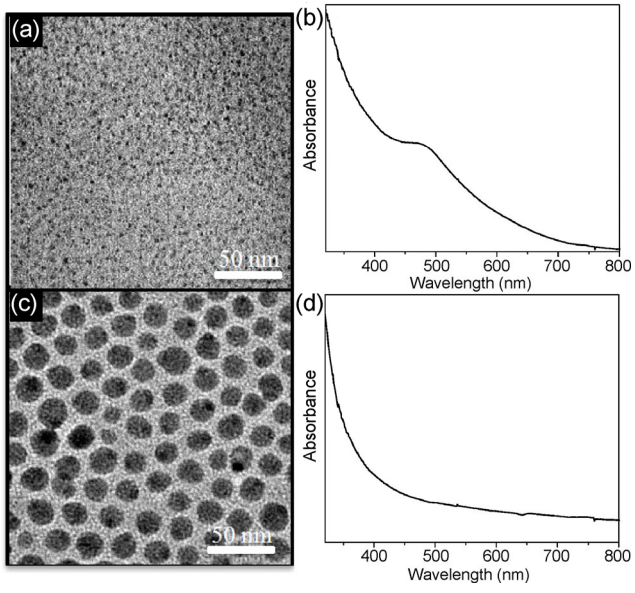

Figure 4 TEM images and UV–vis absorption spectra of ((a) and (b)) the as-prepared $Ag_{16}(GSH)_9$ NC precursors and ((c) and (d)) the as-synthesized Ag_2S NPs.

image indicates the average size of $Ag_{16}(GSH)_9$ was below 2 nm (Fig. 4(a)). The corresponding UV–vis absorption spectrum showed a broad peak at 490 nm (Fig. 4(b)).

By using $Ag_{16}(GSH)_9$ as the precursor in the phase-transfer assisted synthesis, highly monodisperse Ag_2S NPs were also formed, as shown in Fig. 4(c). The UV–vis absorption spectrum of the Ag_2S NPs (Fig. 4(d)) is featureless and lacks the characteristic absorption of $Ag_{16}(GSH)_9$ NCs at ~490 nm, indicating the complete conversion of Ag NCs to Ag_2S NPs.

4 Conclusions

In summary, by using Ag NCs capped with anionic thiolate ligands as precursors, we developed a phase-transfer-assisted route for the synthesis of monodisperse Ag_2S NPs with tunable sizes and surface chemistry. The key in this strategy is to shape the reaction between Ag_{44}(p-MBA)$_{30}$ NCs and S into a uniform, mild, and controllable environment, by the use of the atomic monodispersity and surface chemistry of Ag_{44}(p-MBA)$_{30}$ NCs. The formation of a removable monolayer of CTA^+ on the surface of Ag_{44}(p-MBA)$_{30}$ NCs contributed significantly to the regulation of the growth kinetics of Ag_2S NPs, and also allowed the more difficult aqueous synthesis to be bypassed. Ag_2S NPs synthesized in this way were monodisperse, size-tunable (4–16 nm), and had controllable surface chemistry (switchable solubility between aqueous and organic solvents via a simple cation-exchange reaction). This research is interesting, not only because the obtained highly monodisperse Ag_2S NPs are attractive for further applications, but also because the protocol developed in this study exemplified the usefulness of the supramolecular chemistry of metal NCs in the preparation of high quality chalcogenide NPs, which may offer an efficient route for the preparation of other semiconductors.

Acknowledgements

This work is financially supported by the National Natural Science Foundation of China (Nos. 21173226, 21376247, and 21573240), and the Ministry of Education, Singapore (No. R-279-000-409-112).

Electronic Supplementary Material: Supplementary material (XPS, EDX, FTIR and photograph of the samples) is available in the online version of this article at http://dx.doi.org/10.1007/s12274-015-0980-y.

References

[1] Lim, W. P.; Zhang, Z. H.; Low, H. Y.; Chin, W. S. Preparation of Ag_2S nanocrystals of predictable shape and size. *Angew. Chem., Int. Ed.* **2004**, *43*, 5685–5689.

[2] Lou, W. J.; Wang, X. B.; Chen, M.; Liu, W. M.; Hao, J. C. A simple route to synthesize size-controlled Ag_2S core–shell nanocrystals, and their self-assembly. *Nanotechnology* **2008**, *19*, 225607.

[3] Du, Y. P.; Xu, B.; Fu, T.; Cai, M.; Li, F.; Zhang, Y.; Wang, Q. B. Near-infrared photoluminescent Ag_2S quantum dots from a single source precursor. *J. Am. Chem. Soc.* **2010**, *132*, 1470–1471.

[4] Shen, S. L.; Zhang, Y. J.; Peng, L.; Du, Y. P.; Wang, Q. B. Matchstick-shaped Ag_2S–ZnS heteronanostructures preserving both UV/blue and near-infrared photoluminescence. *Angew. Chem., Int. Ed.* **2011**, *50*, 7115–7118.

[5] Zhang, Y.; Hong, G. S.; Zhang, Y. J.; Chen, G. C.; Li, F.; Dai, H. J.; Wang, Q. B. Ag_2S quantum dot: A bright and biocompatible fluorescent nanoprobe in the second near-infrared window. *ACS Nano* **2012**, *6*, 3695–3702.

[6] Yang, J.; Ying, J. Y. Nanocomposites of Ag_2S and noble metals. *Angew. Chem., Int. Ed.* **2011**, *50*, 4637–4643.

[7] Wang, D. S.; Xie, T.; Peng, Q.; Li, Y. Ag, Ag_2S, and Ag_2Se nanocrystals: Synthesis, assembly, and construction of mesoporous structures. *J. Am. Chem. Soc.* **2008**, *130*, 4016–4022.

[8] Yang, J.; Ying, J. Y. A general phase-transfer protocol for metal ions and its application in nanocrystal synthesis. *Nat. Mater.* **2009**, *8*, 683–689.

[9] Zhu, G. X.; Xu, Z. Controllable growth of semiconductor heterostructures mediated by bifunctional Ag_2S nanocrystals as catalyst or source-host. *J. Am. Chem. Soc.* **2011**, *133*, 148–157.

[10] Brelle, M. C.; Zhang, J. Z.; Nguyen, L.; Mehra, R. K. Synthesis and ultrafast study of cysteine- and glutathione-capped Ag_2S semiconductor colloidal nanoparticles. *J. Phys. Chem. A* **1999**, *103*, 10194–10201.

[11] Yang, L.; Xing, R. M.; Shen, Q. M.; Jiang, K.; Ye, F.; Wang, J. Y.; Ren, Q. S. Fabrication of protein-conjugated silver sulfide nanorods in the bovine serum albumin solution. *J. Phys. Chem. B* **2006**, *110*, 10534–10539.

[12] Mo, X.; Krebs, M. P.; Yu, S. M. Directed synthesis and

assembly of nanoparticles using purple membrane. *Small* **2006**, *2*, 526–529.

[13] Jin, R. C. Quantum sized, thiolate-protected gold nanoclusters. *Nanoscale* **2010**, *2*, 343–362.

[14] Lu, Y. Z.; Chen, W. Sub-nanometre sized metal clusters: From synthetic challenges to the unique property discoveries. *Chem. Soc. Rev.* **2012**, *41*, 3594–3623.

[15] Negishi, Y.; Nobusada K.; Tsukuda, T. Glutathione-protected gold clusters revisited: Bridging the gap between gold(I)−thiolate complexes and thiolate-protected gold nanocrystals. *J. Am. Chem. Soc.* **2005**, *127*, 5261−5270.

[16] Zheng, J.; Nicovich P. R.; Dickson, R. M. Highly fluorescent noble-metal quantum dots. *Annu. Rev. Phys. Chem.* **2007**, *58*, 409–431.

[17] Chen, S. W.; Ingram, R. S.; Hostetler, M. J.; Pietron, J. J.; Murray, R. W.; Schaaff, T. G.; Khoury, J. T.; Alvarez M. M.; Whetten, R. L. Gold nanoelectrodes of varied size: Transition to molecule-like charging. *Science* **1998**, *280*, 2098–2101.

[18] Luo, Z. T.; Zheng, K. Y.; Xie, J. P. Engineering ultrasmall water-soluble gold and silver nanoclusters for biomedical applications. *Chem. Commun.* **2014**, *50*, 5143–5155.

[19] Yuan, X.; Setyawati, M. I.; Tan, A. S.; Ong, C. N.; Leong, D. T.; Xie, J. P. Highly luminescent silver nanoclusters with tunable emissions: Cyclic reduction–decomposition synthesis and antimicrobial properties. *NPG Asia Mater.* **2013**, *5*, e39.

[20] Yamazoe, S.; Koyasu K.; Tsukuda, T. Nonscalable oxidation catalysis of gold clusters. *Acc. Chem. Res.* **2014**, *47*, 816–824.

[21] Dass, A.; Theivendran, S.; Nimmala, P. R.; Kumara, C.; Jupally, V. R.; Fortunelli, A.; Sementa, L.; Barcaro, G.; Zuo, X.; Noll, B. C. $Au_{133}(SPh\text{-}tBu)_{52}$ nanomolecules: X-ray crystallography, optical, electrochemical, and theoretical analysis. *J. Am. Chem. Soc.* **2015**, *137*, 4610–4613.

[22] Yuan, X.; Luo, Z. T.; Yu, Y.; Yao, Q. F.; Xie, J. P. Luminescent noble metal nanoclusters as an emerging optical probe for sensor development. *Chem.—Asian J.* **2013**, *8*, 858–871.

[23] Choi, S.; Park, S.; Yu, J. H. Ligand-assisted etching: The stability of silver nanoparticles and the generation of luminescent silver nanodots. *Chem. Commun.* **2014**, *50*, 15098–15100.

[24] Jin, R. C.; Qian, H. F.; Wu, Z. K.; Zhu, Y.; Zhu, M. Z.; Mohanty, A.; Garg, N. Size focusing: A methodology for synthesizing atomically precise gold nanoclusters. *J. Phys. Chem. Lett.* **2010**, *1*, 2903–2910.

[25] Yu, Y.; Yao, Q. F.; Luo, Z. T.; Yuan, X.; Lee, J. Y.; Xie, J. P. Precursor engineering and controlled conversion for the synthesis of monodisperse thiolate-protected metal nanoclusters. *Nanoscale* **2013**, *5*, 4606–4620.

[26] Wang, S. X.; Song, Y. B.; Jin, S.; Liu, X.; Zhang, J.; Pei, Y.; Meng, X. M.; Chen, M.; Li, P.; Zhu, M. Z. Metal exchange method using Au_{25} nanoclusters as templates for alloy nanoclusters with atomic precision. *J. Am. Chem. Soc.* **2015**, *137*, 4018–4021.

[27] Luo, Z. T.; Nachammai, V.; Zhang, B.; Yan, N.; Leong, D. T.; Jiang, D.-E.; Xie, J. P. Toward understanding the growth mechanism: Tracing all stable intermediate species from reduction of Au(I)–thiolate complexes to evolution of Au_{25} nanoclusters. *J. Am. Chem. Soc.* **2014**, *136*, 10577−10580.

[28] Kurashige, W.; Niihori, Y.; Sharma, S.; Negishi, Y. Recent progress in the functionalization methods of thiolate-protected gold clusters. *J. Phys. Chem. Lett.* **2014**, *5*, 4134–4142.

[29] Wang, Y.; Su, H. F.; Xu, C. F.; Li, G.; Gell, L.; Lin, S. C.; Tang, Z. C.; Häkkinen, H.; Zheng, N. F. An intermetallic $Au_{24}Ag_{20}$ superatom nanocluster stabilized by labile ligands. *J. Am. Chem. Soc.* **2015**, *137*, 4324–4327.

[30] AbdulHalim, L. G.; Kothalawala, N.; Sinatra, L.; Dass, A.; Bakr, O. M. Neat and complete: Thiolate-ligand exchange on a silver molecular nanoparticle. *J. Am. Chem. Soc.* **2014**, *136*, 15865−15868.

[31] Yao, C. H.; Chen, J. S.; Li, M.-B.; Liu, L. R.; Yang, J. L.; Wu, Z. K. Adding two active silver atoms on Au_{25} nanoparticle. *Nano Lett.* **2015**, *15*, 1281−1287.

[32] Yuan, X.; Zhang, B.; Luo, Z. T.; Yao, Q. F.; Leong, D. T.; Yan, N.; Xie, J. P. Balancing the rate of cluster growth and etching for gram-scale synthesis of thiolate-protected Au_{25} nanoclusters with atomic precision. *Angew. Chem., Int. Ed.* **2014**, *53*, 4623–4627.

[33] Desireddy, A.; Conn, B. E.; Guo, J. S.; Yoon, B.; Barnett, R. N.; Monahan, B. M.; Kirschbaum, K.; Griffith, W. P.; Whetten, R. L.; Landman, U. et al. Ultrastable silver nanoparticles. *Nature* **2013**, *501*, 399–402.

[34] Yao, Q. F.; Yu, Y.; Yuan, X.; Zhao, D.; Xie, J. P.; Lee, J. Y. Counterion-assisted shaping of nanocluster supracrystals. *Angew. Chem., Int. Ed.* **2015**, *54*, 184–189.

[35] Yao, Q. F.; Yuan, X.; Yu, Y.; Xie, J. P.; Lee, J. Y. Introducing amphiphilicity to noble metal nanoclusters via phase-transfer driven ion-pairing reaction. *J. Am. Chem. Soc.* **2015**, *137*, 2128–2132.

[36] Bakr, O. M.; Amendola, V.; Aikens, C. M.; Wenseleers, W.; Li, R.; Dal Negro, L.; Schatz, G. C.; Stellacci, F. Silver nanoparticles with broad multiband linear optical absorption. *Angew. Chem., Int. Ed.* **2009**, *48*, 5921–5926.

[37] Yang, H. Y.; Zhao, Y. W.; Zhang, Z. Y.; Xiong, H. M.; Yu, S. N. One-pot synthesis of water-dispersible Ag_2S quantum dots with bright fluorescent emission in the second near-infrared window. *Nanotechnology* **2013**, *24*, 055706.

[38] Martínez-Castañón, G. A.; Sánchez-Loredo, M. G.; Dorantes, H. J.; Martínez-Mendoza, J. R.; Ortega-Zarzosa, G.; Ruiz, F. Characterization of silver sulfide nanoparticles synthesized by a simple precipitation method. *Mater. Lett.* **2005**, *59*, 529–534.

[39] Ma, D. K.; Hu, X. K.; Zhou, H. Y.; Zhang, J. H.; Qian, Y. T. Shape-controlled synthesis and formation mechanism of nanoparticles-assembled Ag_2S nanorods and nanotubes. *J. Cryst. Growth* **2007**, *304*, 163–168.

[40] Zhao, Y. B.; Zhang, D. W.; Shi, W. F.; Wang, F. A gamma-ray irradiation reduction route to prepare rod-like Ag_2S nanocrystallines at room temperature. *Mater. Lett.* **2007**, *61*, 3232–3234.